









Complex magnetic behavior in $\text{Ho}_2\text{Re}_3\text{Si}_5$ single crystalVikash Sharma , Shovan Dan , Suman Nandi , Gourav Dwari , Bishal Baran Maity , Suman Sanki ,
Ruta Kulkarni , and A. Thamizhavel ^{*}*Department of Condensed Matter Physics and Materials Science, Tata Institute of Fundamental Research, Homi Bhabha Road, Colaba, Mumbai-400005, India*

(Received 1 July 2022; revised 6 November 2022; accepted 21 November 2022; published 14 December 2022)

We report on the magnetic, electrical transport, and thermal properties of $\text{Ho}_2\text{Re}_3\text{Si}_5$ single crystal by means of magnetization, electrical resistivity, and heat capacity measurements in the temperature range 2–300 K. Magnetic susceptibility, heat capacity, and electrical resistivity reveal two closely spaced antiferromagnetic transitions at $T_{N1} \sim 3.8$ K and $T_{N2} \sim 4.2$ K. Three field-induced metamagnetic transitions at 4.5, 10, and 15 kOe, in the magnetically ordered state at 2 K, have been observed, in the isothermal magnetization, for $\mu_0 H \parallel c$, and their first-order nature is evident from the magnetic hysteresis. The hysteresis disappears and metamagnetic transitions become feeble at around 3.5 K. These metamagnetic transitions are consistent with field-induced magnetic phases as observed in the magnetic susceptibility, electrical resistivity, and heat capacity. The magnetization for $\mu_0 H \parallel a$ is linear without any signature of metamagnetic transition for fields up to 70 kOe suggesting the hard axis of magnetization. From the temperature dependence of the isothermal magnetization, we have constructed a magnetic phase diagram, which signals a complex magnetic structure in this compound. These results suggest that magnetic and transport properties are highly sensitive to the external magnetic field.

DOI: [10.1103/PhysRevMaterials.6.124406](https://doi.org/10.1103/PhysRevMaterials.6.124406)

I. INTRODUCTION

The rare-earth intermetallic compounds possessing the stoichiometry $R_2T_3X_5$, where R is a rare earth, T is a transition metal, and X is a group IV element, exhibit interesting physical properties [1–6]. For instance, the Kondo and heavy fermion behavior in $\text{Ce}_2(\text{Rh}, \text{Ir})_3\text{Ge}_5$ and $\text{Pr}_2\text{Pd}_3\text{Ge}_5$ [7,8], valence fluctuation in $\text{Ce}_2\text{Re}_3\text{Si}_5$ [9], charge density wave (CDW) transition in $\text{Er}_2\text{Ir}_3\text{Si}_5$ and $\text{Lu}_2\text{Ir}_3\text{Si}_5$ [6,10], and pressure-induced superconductivity in $\text{Ce}_2\text{Ni}_3\text{Ge}_5$ [11] have been reported. These $R_2T_3X_5$ compounds usually adopts either $\text{U}_2\text{Co}_3\text{Si}_5$ -type orthorhombic crystal structure with the space group $Ibam$ [4] or $\text{U}_2\text{Mn}_3\text{Si}_5$ -type tetragonal crystal structure with the space group $P4/mnc$ [12]. Although there exist some reports on physical properties of orthorhombic $R_2T_3X_5$ ($T = \text{Mn}, \text{Co}, \text{Pt}, \text{Pd}, \text{Rh}, \text{Ir}$) [3,4,6–8,10], while properties of tetragonal $R_2T_3X_5$ ($T = \text{Fe}, \text{Re}, \text{Os}$) are not well explored [9]. Recently, we have reported the anisotropic magnetic properties of $R_2\text{Re}_3\text{Si}_5$ ($R = \text{Ce}$ and Pr) single crystals [9]. The $\text{Ce}_2\text{Re}_3\text{Si}_5$ showed intermediate valence state as evident from x-ray photoelectron spectroscopy (XPS) and magnetic susceptibility (χ). The $\text{Pr}_2\text{Re}_3\text{Si}_5$ showed a sharp drop in the χ at ~ 9 K and a spin-flip-like metamagnetic transition near 35 kOe for $\mu_0 H \parallel c$ in the plot of magnetization (M) versus field, which suggested an Ising-type antiferromagnetic (AFM) ordering at $T_N \sim 9$ K [9]. The anisotropic magnetic properties of $\text{Pr}_2\text{Re}_3\text{Si}_5$ have been explained by the crystalline electric field (CEF) effect based on a point charge model. The CEF analysis suggests that the ninefold degenerate ($2J + 1$)

ground state splits into 9 levels with an overall splitting of 1179 K.

In the present work, our aim is to explore the anisotropic properties of a new member of $R_2\text{Re}_3\text{Si}_5$ family. Therefore, we have synthesized a single crystal of $\text{Ho}_2\text{Re}_3\text{Si}_5$, and investigated its magnetic, electrical and thermal transport properties by using χ , M , heat capacity (C_p), and electrical resistivity (ρ). These properties are measured on a well-aligned single crystal along the two main crystallographic directions, viz., a and c axes. Significant anisotropy along a - and c axes in χ , M and ρ has been observed. The χ , C_p , and ρ reveal two magnetic phase transitions at $T_{N1} \sim 3.8$ K and $T_{N2} \sim 4.2$ K, which are associated with long-range AFM ordering. The T_{N2} is significantly weaker compared to T_{N1} . We have also observed field-induced first-order metamagnetic transitions near 4, 10, and 15 kOe at 2 K in the plot of $M(H)$ measured along c axis. In contrast to two magnetic transitions T_{N1} and T_{N2} and three metamagnetic transitions in $\text{Ho}_2\text{Re}_3\text{Si}_5$, its isostructural compound $\text{Pr}_2\text{Re}_3\text{Si}_5$ shows only one magnetic transition $T_N \sim 9$ K, and one field-induced metamagnetic transition about 3.5 T [9]. Therefore, magnetic and transport properties of $\text{Ho}_2\text{Re}_3\text{Si}_5$ modify in complicated ways with the application of magnetic field. We have constructed the phase diagram from the temperature dependence of the isothermal magnetization.

II. EXPERIMENTAL METHODS

$\text{Ho}_2\text{Re}_3\text{Si}_5$ single crystal was prepared directly from its melt by Czochralski method in a tetra-arc furnace (Technosearch Corporation, Japan) under ultrapure argon atmosphere. The high purity starting elements of Ho, Re, and Si in the molar ratio of 2:3:5 were melted to prepare a poly-

^{*}thamizh@tifr.res.in

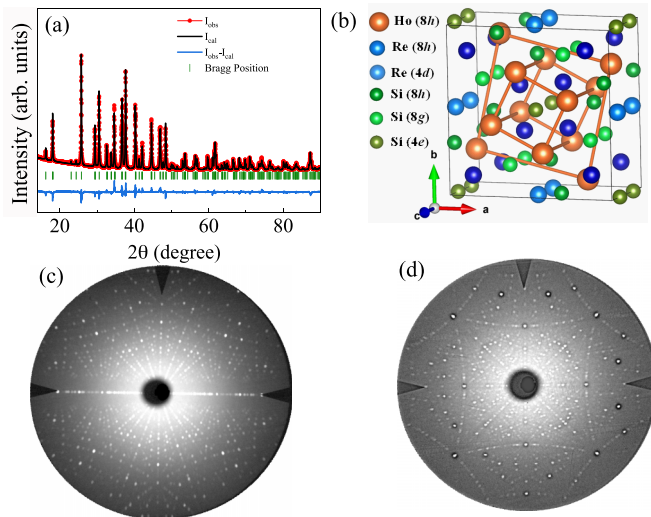


FIG. 1. (a) Powder x-ray diffraction along with Rietveld-refinement, (b) crystal structure, and [(c) and (d)] Laue diffraction patterns corresponding to the (110) and (001) planes of $\text{Ho}_2\text{Re}_3\text{Si}_5$.

crystalline ingot of $\text{Ho}_2\text{Re}_3\text{Si}_5$. The melting process was done for three times to make it homogeneous. A seed crystal was cut from this polycrystalline ingot, and this seed was inserted into the molten solution and pulled rapidly at a speed of 50 mm/h. After attaining the steady state condition, the pulling speed was reduced to 10 mm/h for the entire growth of the single crystal. A small portion of the crystal was ground to make fine powder, and subjected to room-temperature x-ray diffraction (XRD) to check the phase purity.

PANalytical x-ray diffractometer equipped with a $\text{Cu } K_\alpha$ monochromatic source with wavelength $\lambda = 1.5406 \text{ \AA}$ was used for XRD. The obtained single crystal was oriented using Laue method of XRD in back reflection geometry. It was cut along the two principal crystallographic axes viz., a and c by a wire electric discharge machine. Field emission scanning electron microscope (FESEM) Zeiss ULTRA plus equipped with energy dispersive x-ray (EDX) spectrometer was used to determine the composition of the grown crystal. Magnetic measurements were performed using a superconducting quantum interference device - vibrating sample magnetometer (SQUID-VSM), Quantum Design, USA. Electrical and thermal transport measurements were performed in a physical property measurement system (PPMS), Quantum Design, USA. The electrical resistivity was measured by the

four-probe method by passing the current along the a and c axes of the oriented single crystals. Gold wire with diameter of $40 \mu\text{m}$ was used to make electrical contacts using silver paste to the crystal surface.

III. RESULTS AND DISCUSSION

A. Structural study

Figure 1(a) shows the XRD pattern of powder sample obtained from a finely ground piece of grown crystal along with the Rietveld refinement. The FULLPROF software package was used to refine the x-ray powder diffraction data [13]. Rietveld analysis reveals that $\text{Ho}_2\text{Re}_3\text{Si}_5$ crystallizes in the $\text{U}_2\text{Mn}_3\text{Si}_5$ -type tetragonal crystal structure with the space group $P4/mnc$ (No. 128). The obtained lattice parameters are $a = 10.922(1) \text{ \AA}$ and $c = 5.494(1) \text{ \AA}$, and the unit cell volume is $655.50(3) \text{ \AA}^3$. The refined atomic coordinates are listed in Table I. Lattice parameters and unit cell volume are found to be smaller compared to $\text{Pr}_2\text{Re}_3\text{Si}_5$ which is expected due to the lanthanide contraction [9]. The crystal structure of $\text{Ho}_2\text{Re}_3\text{Si}_5$ is shown in Fig. 1(b). It shows that Ho atoms in the unit cell are arranged in a rectangular network with a nearest neighboring distance of $3.852(3) \text{ \AA}$. The Ho atom has only one site with $8h$ Wyckoff's position, Re atoms occupy two different $8h$ and $4d$ Wyckoff's positions, and Si atoms occupy three different $8h$, $8g$, and $4e$ Wyckoff's positions. The Laue diffraction patterns corresponding to planes, viz., (110) and (001) are shown in Figs. 1(c) and 1(d), respectively. Well defined Laue diffraction spots indicate the good quality of the grown single crystal. Energy dispersive analysis of x rays confirms the 2:3:5 ratio of atomic percentage of Ho, Re, Si, respectively, which is not shown here for brevity.

B. Magnetic properties

The temperature-dependent χ measured in an applied magnetic field of 50 Oe, along the a and c axes, namely, χ_a and χ_c , respectively, are shown in Fig. 2(a). The χ measured under zero-field-cooled (ZFC) and FC show reversibility, and hence we showed only FC data. Both χ_a and χ_c show an anomaly near $T_{N1} \approx 3.8 \text{ K}$, which is associated with AFM ordering. Note that there is change in slope at $T_{N2} \approx 4.2 \text{ K}$ [Fig. 2(a) and inset]. Further to see the nature of these transitions, we have measured χ_a and χ_c in an applied magnetic field of 2 kOe [Fig. 2(b)] in the temperature range 1.8 to 300 K. The χ_a increases with decrease in temperature with a broad hump between 25 to 200 K, and there is a sharp drop in

TABLE I. Refined structural parameters and agreement factors for $\text{Ho}_2\text{Re}_3\text{Si}_5$ obtained from Rietveld refinement of powder x-ray diffraction pattern using tetragonal space group $P4/mnc$.

Atoms	Wyck	x	y	z	$B(\text{\AA}^2)$
Ho	$8h$	0.262(2)	0.421(3)	0.000	1.1(1)
Re1	$8h$	0.146(3)	0.122(4)	0.000	0.5 (1)
Re2	$4d$	0.000	0.500	0.250	0.3 (2)
Si1	$8h$	0.034(5)	0.310(4)	0.000	0.2 (1)
Si2	$8g$	0.170(3)	0.670(3)	0.250	0.2 (2)
Si3	$4e$	0.000	0.000	0.273(6)	0.3 (1)
$a = b = 10.922(1) \text{ \AA}$		$c = 5.494(1) \text{ \AA}$		$V = 655.50(3) \text{ \AA}^3$	$R_p: 13.7, R_{wp}: 14.1, R_{\text{expt}}: 3.16, \chi^2: 15.9$

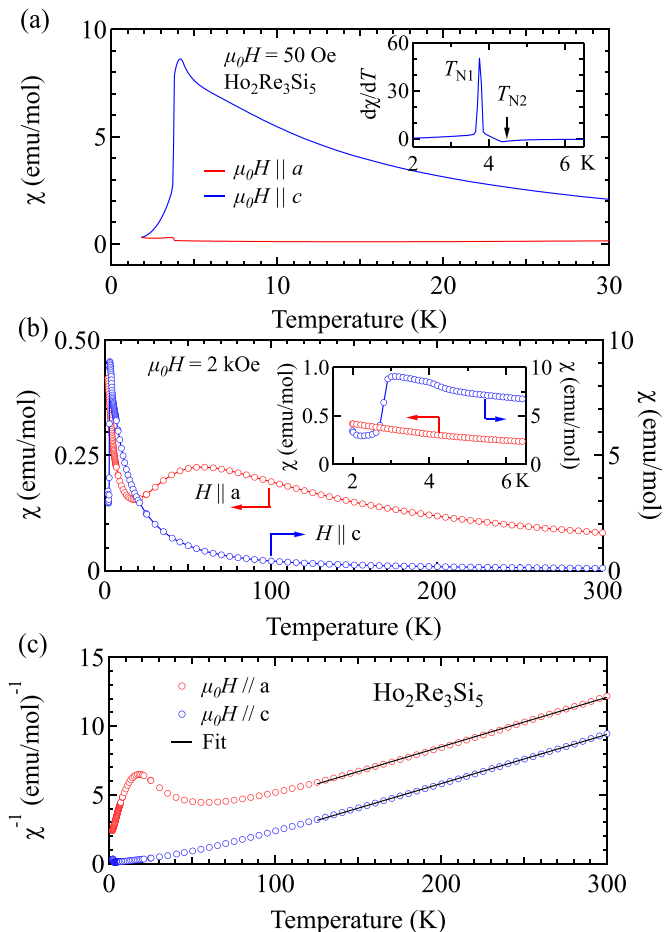


FIG. 2. (a) Temperature-dependent magnetic susceptibility of $\text{Ho}_2\text{Re}_3\text{Si}_5$ along a and c directions measured at 50 Oe, inset shows derivative plot at low temperatures, (b) 2 kOe data, inset shows expanded view of the low-temperature region, and (c) inverse susceptibility of 2 kOe data; the solid lines are fits to the Curie-Weiss law.

the susceptibility at $T_{N1} \approx 3.8$ K [Fig. 2(b)]. The broad hump observed in the temperature range 25 to 200 K is most likely due to higher-lying crystal electric field (CEF) states that are populated by thermal energy $k_B T$ [14]. A completely distinct behavior of χ_c compared to χ_a is found. The χ_c , below 100 K, increases with decrease in temperature with change

in slope at $T_{N2} \approx 4$ K, and attains the peak at $T_{N1} \approx 3.1$ K where it sharply drops about 3.5 times of the peak value [Fig. 2(b)]. These closely spaced transitions are associated with AFM transitions as observed in the low field of 50 Oe. Notably, the transitions at $T_{N1} \approx 3.8$ K and $T_{N2} \approx 4.2$ K are found in 50 Oe, and are highly sensitive to applied magnetic field [Fig. 2(a) and inset]. The inset of Fig. 2(b) depicts the low-temperature region of the 2 kOe data along the easy axis direction, namely, $\mu_0 H \parallel c$. These features are also reflected in electrical and thermal transport measurements for $\mu_0 H \parallel c$, and hence we shall revisit thoroughly in text.

We have analysed the inverse susceptibility χ_a^{-1} and χ_c^{-1} using the Curie Weiss (CW) law defined as $\chi = \mu_{\text{eff}}^2 n / (8(T - \theta_p))$, where n is the number of rare-earth atoms (2 in this case), and θ_p is the paramagnetic Weiss temperature, in the temperature range 120–300 K [Fig. 2(c)]. The μ_{eff} along a - and c -directions are found to be about 10.54 and 10.56 μ_B/Ho , respectively which is close to the theoretical value of 10.63 μ_B/Ho of free Ho^{3+} (for Ho^{3+} , $J = 8.0$ and $g_J = 5/4$; $\mu_{\text{eff}} = g_J \sqrt{J(J+1)} = 10.63 \mu_B$). The θ_p in a and c axes are found to be about -35.5 and 37.2 K, respectively. We also estimated the magnetic frustration ratio $f = (\theta_p/T_N)$, which is found to be ~ 9.3 for a axis. This indicates that significant spin frustration along a axis. The ratio of susceptibilities along c and a axes i.e., χ_c/χ_a at T_{N1} is about 15. These results, therefore, clearly indicate that magnetic properties in this compound are highly anisotropic which results from the CEF splitting of the ground state multiplet of the degenerate ($J = 8$; $(2J + 1) = 17$) levels of the Ho^{3+} ion.

Now we turn our discussion on field-induced magnetic phases in $\text{Ho}_2\text{Re}_3\text{Si}_5$. The field-dependent χ_c is shown in Figs. 3(a)–3(c). As the field increases, T_{N1} shifts from ~ 3.8 to ~ 3.1 K up to 2 kOe [Fig. 3(a)]. The χ_c sharply increases for applied magnetic fields of 1 and 1.5 kOe at 4.2 K. Notably, the χ_c shows an upturn at ~ 2.2 K, which may be due to the field induced transition as observed in the $M(H)$ data. At 4 kOe, T_{N2} completely disappears, while T_{N1} still survives with slight shift towards higher temperature. The disappearance of T_{N2} can be correlated with field-induced first metamagnetic transition at $\mu_0 H_{c1} = 3.9$ kOe, as discussed later [Fig. 4(a)]. The χ_c drops again at ~ 3.9 K and raises at ~ 3.6 K in 5.5 kOe. This broad hump seems to associate with both T_{N1} and T_{N2} . Note that these transitions are closely spaced and become broader with the increase in applied magnetic field and hence it is difficult to resolve them. With further increase in field, this

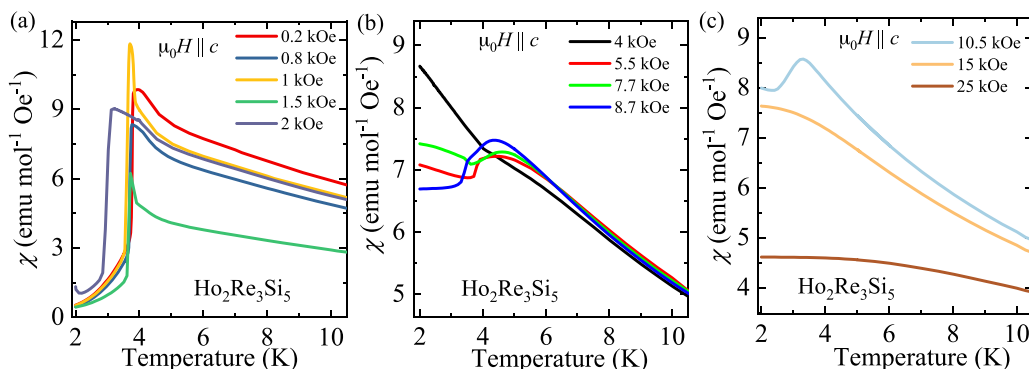


FIG. 3. [(a)–(c)] Magnetic susceptibility of $\text{Ho}_2\text{Re}_3\text{Si}_5$ along c axis at different applied magnetic fields.

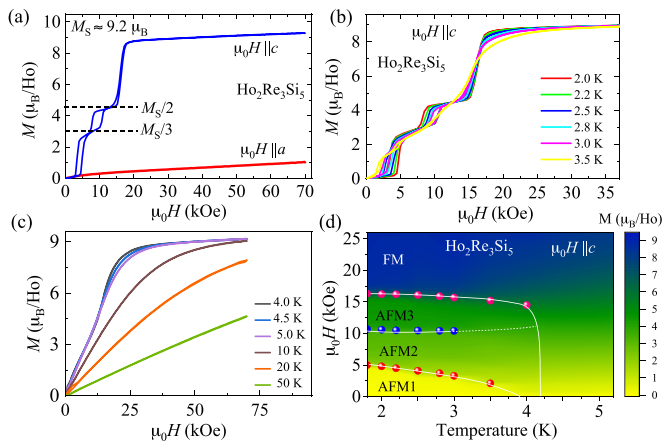


FIG. 4. (a) Magnetization along the two principal crystallographic axes, a and c measured at $T = 2$ K, [(b) and (c)] magnetization at different temperatures along c axis, and (d) magnetic phase diagram constructed from magnetization data of $\text{Ho}_2\text{Re}_3\text{Si}_5$, the scale bar shows the moment (μ_B/Ho), the solid lines are guide to the eyes.

broad hump more or less shifts towards higher temperature up to 8.7 kOe, and towards lower temperature at 10.5 kOe. Above 15 kOe, it shows a field-induced ferromagnetic-like behavior as evident from the clear suppression of broad hump. This complex magnetic behavior of $\text{Ho}_2\text{Re}_3\text{Si}_5$ in χ_c is mainly attributed to modification of magnetic structure due to applied magnetic fields in a complicated way as evident from magnetization along c axis [Fig. 4(b)]. Figure 4(a) shows isothermal magnetization along the a and c axes, namely, M_a and M_c , respectively measured at $T = 2$ K, in the magnetically ordered state. The M_c clearly shows three metamagnetic transitions at $\mu_0 H_{c1} = 4$ kOe, $\mu_0 H_{c2} = 10$ kOe, and $\mu_0 H_{c3} = 15$ kOe corresponding to magnetization jumps of $M_s/54 \approx 0.17\mu_B$, $M_s/3 \approx 3.1\mu_B$, and $M_s/2 \approx 4.57\mu_B$, where $M_s \approx 9.2\mu_B/\text{Ho}$ is the saturated magnetic moment obtained at 2 K and 70 kOe. The M_s is close to the expected saturated magnetic moment of $10.6\mu_B/\text{Ho}$ for a free Ho^{3+} ion. The significant hysteresis in M_c confirms the first order nature of these metamagnetic transitions. Unlike the M_c , M_a does not show any metamagnetic transition, and no signature of saturation even up to 70 kOe. This indicates that a axis is the hard axis while c is the easy axis of magnetization. The ratio of magnetization measured along c and a axis M_c/M_a is ≈ 9 at 70 kOe. These results clearly indicate that there is a strong magnetocrystalline anisotropy in $\text{Ho}_2\text{Re}_3\text{Si}_5$.

From the M_c plot, we can consider four different magnetic phases in $\text{Ho}_2\text{Re}_3\text{Si}_5$. Three of them are AFM phases, AFM1 for $0 < \mu_0 H_{c1} < 4$ kOe, AFM2 for $5.5 < \mu_0 H_{c2} < 10$ kOe and AFM3 for $11 < \mu_0 H_{c3} < 15$ kOe, and fourth is a field-induced ferromagnetic state for $\mu_0 H_{c3} > 15$ kOe. The first plateau between 5 to 10 kOe has a magnetization of $\sim M_s/3$, and second plateau between 11 to 15 kOe has a magnetization of $\sim M_s/2$. These results indicate a complex magnetic structure in applied magnetic fields. The first plateau has magnetization of $M_s/3$, i.e., AFM2 phase. Such plateau at one-third of M_s with the same spin arrangement has been reported in tetragonal $\text{HoNi}_2\text{B}_2\text{C}$ [15,16] and $\text{UAu}_{0.8}\text{Sb}_2$ [17].

The exact spin configurations of these field-induced phases may be difficult to infer from the present set of data and hence it warrants the microscopic technique like neutron diffraction studies, which is planned for the future.

In order to see the temperature dependence on metamagnetic transitions, we have measured M_c at different temperatures [Figs. 4(b) and 4(c)]. The coercivity of hysteresis across metamagnetic transitions and M_s gradually suppresses with increase in temperature [Fig. 4(b)]. The hysteresis disappears and metamagnetic transitions become feeble at 3.5 K. Although metamagnetic transitions completely disappear at $T = 5$ K, the magnetization along c axis still shows saturation which may be attributed to some short range magnetic interactions above T_N [Fig. 4(c)]. The paramagnetic-like behavior sets in above 20 K. The magnetic phase diagram constructed from M_c data is shown in Fig. 4(d). The temperature dependence of the isothermal magnetization enabled us to construct the magnetic phase diagram of $\text{Ho}_2\text{Re}_3\text{Si}_5$. The constructed phase diagram in the plane of magnetic field and temperature is shown in Fig. 4(d). For T less than 4.2 K and sufficiently low fields, the system is in the AFM1 state and as the applied magnetic field is increased it enters into the AFM2 state and remains there for fields close to 9 kOe. Further increase in the applied magnetic field the system enters into the AFM3 phase beyond 10 kOe and for fields greater than 15 kOe a field induced ferromagnetic state is attained. It shows mainly four phases, namely, AFM1, AFM2, AFM3, and FM, which are shown by color contrast in Fig. 4(d).

Next, we attempted to analyze the magnetic susceptibility and magnetization data based on the point charge model. The Ho atoms in $\text{Ho}_2\text{Re}_3\text{Si}_5$ occupy $8h$ Wyckoff's position and hence possess the point symmetry m which corresponds to monoclinic site symmetry. However, in order to reduce the complexity in the fitting parameters, we have assumed a orthorhombic site symmetry and used the CEF Hamiltonian for orthorhombic site symmetry which is given by

$$\mathcal{H}_{\text{CEF}} = B_2^0 O_2^0 + B_2^2 O_2^2 + B_4^0 O_4^0 + B_4^2 O_4^2 + B_4^4 O_4^4 + B_6^0 O_6^0 + B_6^2 O_6^2 + B_6^4 O_6^4 + B_6^6 O_6^6, \quad (1)$$

where B_i^m and O_i^m are the crystal field parameters and the Steven's operators [18,19], respectively. We have calculated the CEF susceptibility including the molecular field constant (λ) using the following expression:

$$\chi_i^{-1} = \chi_{\text{CEF}i}^{-1} - \lambda_i. \quad (2)$$

The solid lines in Fig. 5(a) are the calculated curves based on the CEF susceptibility, the expression for $\chi_{\text{CEF}i}$ is given in Ref. [9]. The $(2J + 1)$ levels of the degenerate $J = 8$, split into 17 levels with an overall splitting energy of 365 K. The CEF parameters and the obtained energy levels are shown in Fig. 5(c).

The isothermal magnetization data measured at $T = 2$ K has been analysed using the following CEF Hamiltonian:

$$\mathcal{H} = \mathcal{H}_{\text{CEF}} - g_J \mu_B \mathbf{J}_i (H + \lambda_i M_i), \quad (3)$$

where \mathcal{H}_{CEF} is given by Eq. (1) and the second and third terms represent the Zeeman and molecular field terms, respectively. The expression for M_i is given in Ref. [9].

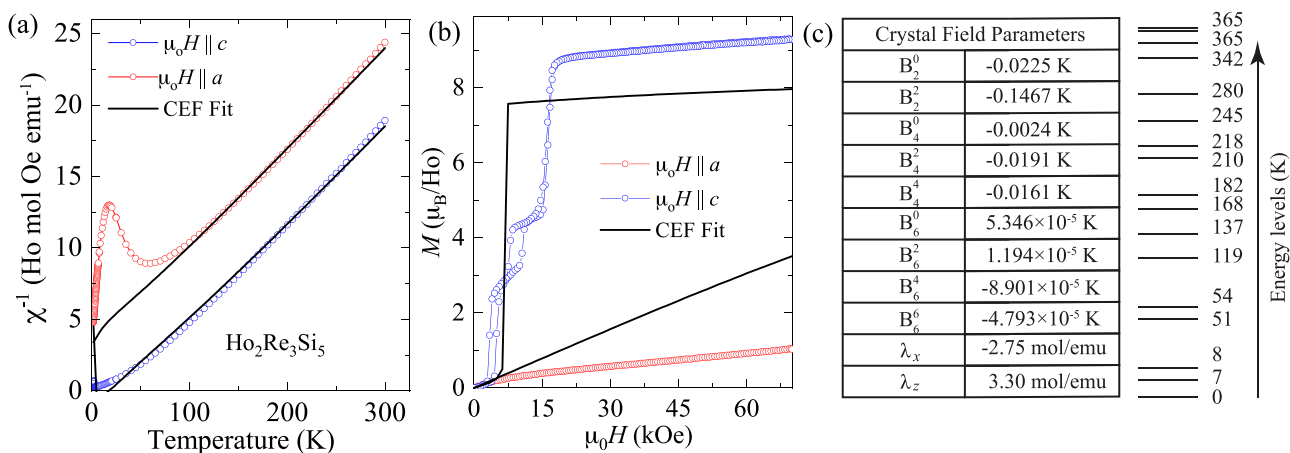


FIG. 5. (a) CEF fit of temperature dependence of the inverse magnetic susceptibility and (b) isothermal magnetization, and (c) energy levels obtained from CEF fitting of $\text{Ho}_2\text{Re}_3\text{Si}_5$

The CEF parameters obtained from the susceptibility fit explains the anisotropy in the magnetization data as well. The solid lines in Fig. 5(b) are the calculated magnetization curves. The discrepancy in the quantitative matching with the experimental data may be attributed to the simplified point charge model. Although the set of parameters explains the anisotropy in the magnetic susceptibility and the magnetization curves, a more detailed study like inelastic neutron diffraction data are essential to know the precise values of the $2J + 1$ degenerate level splitting.

C. Thermal transport properties

The temperature-dependent heat capacity of $\text{Ho}_2\text{Re}_3\text{Si}_5$ is shown in Fig. 6. It shows a λ -like sharp anomaly at $T_{N1} \sim 3.8$ K, and relatively broader and weaker anomaly at $T_{N2} \sim 4.2$ K (Fig. 6, inset). These anomalies correspond to the bulk, long-range AFM ordering in $\text{Ho}_2\text{Re}_3\text{Si}_5$ as observed in χ measurements. The C_p in different magnetic fields applied along c axis is shown in Fig. 7. The T_{N1} and T_{N2} more or

less shift towards lower temperature, and become broader with increasing fields up to 3 kOe. Although a broad peak can be seen at 4 and 5.5 kOe, this peak may correspond to T_{N1} or may have both T_{N1} and T_{N2} . Note that these two transitions are closely spaced, and the field-induced phases set in with the increasing magnetic field. Therefore it is difficult to resolve these closely spaced transitions. The field range between 4 and 5.5 kOe corresponds to AFM1 and AFM2 phases where M_c steadily increases with the applied field [Fig. 4(a)]. However, these transitions get separated again at 7.7 kOe which seem to shift towards higher temperature. This high-temperature shift

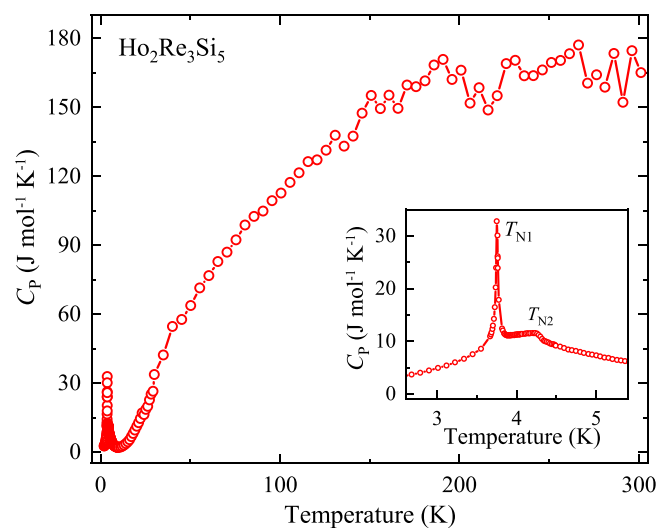


FIG. 6. Temperature-dependent heat capacity of $\text{Ho}_2\text{Re}_3\text{Si}_5$, inset shows the expanded view at low temperature.

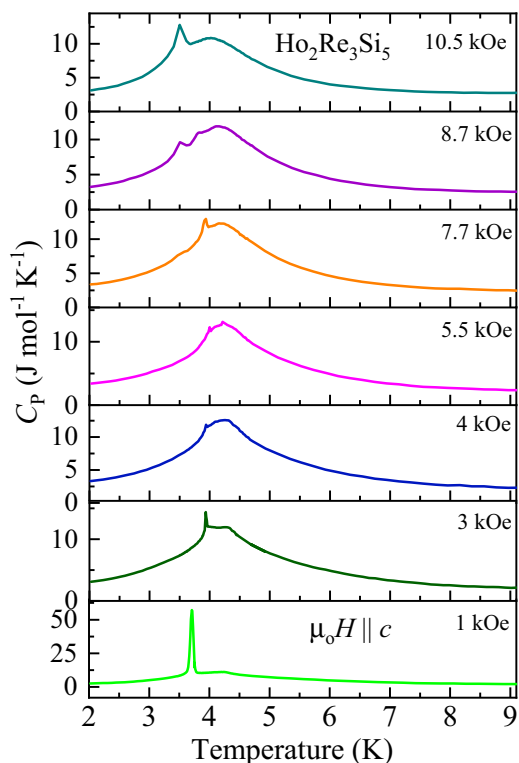


FIG. 7. Temperature-dependent specific heat at different fields applied along the c direction of $\text{Ho}_2\text{Re}_3\text{Si}_5$.

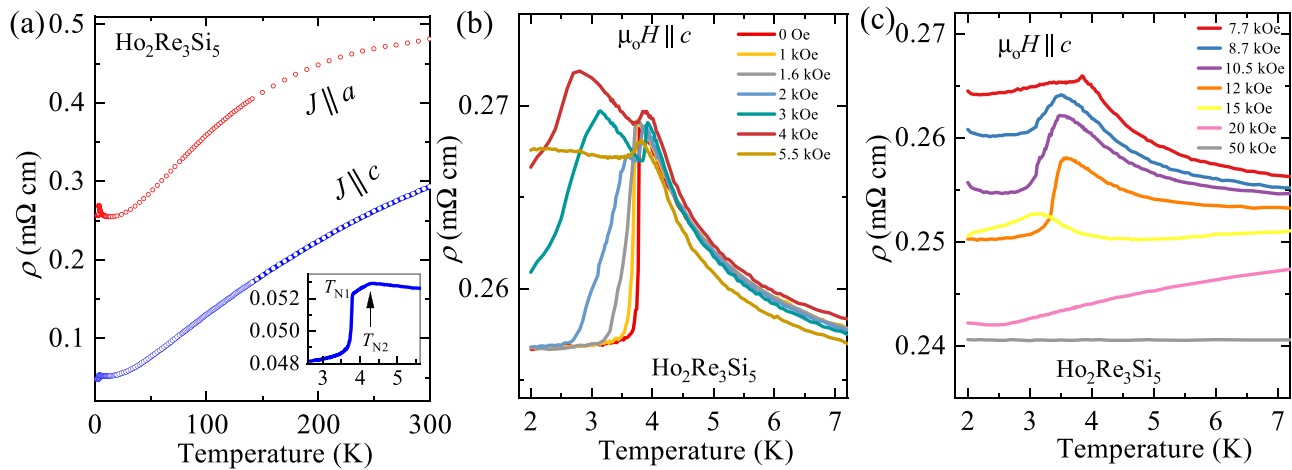


FIG. 8. (a) Temperature-dependent electrical resistivity for $J \parallel a$ and c , inset shows expanded view of resistivity for $J \parallel c$ at low temperature, and (b, c) temperature dependence of resistivity in various applied magnetic fields for $J \parallel a$ and $\mu_0 H \parallel c$.

may be associated with some ferromagnetic interactions in AFM1 and AFM2 phases. Above 8.7 kOe, these transitions shift towards lower temperature which is in line with χ_c data. We would like to emphasize here that this compound shows the complex magnetic behavior which is highly sensitive to an external magnetic field.

D. Electrical transport properties

The temperature-dependent electrical resistivity measured in zero field with current applied along a and c axes are shown in Fig. 8(a). In case of $J \parallel c$, as temperature decreases, $\rho(T)$ decreases down to ~ 11 K and exhibits an overall metallic behavior of $\text{Ho}_2\text{Re}_3\text{Si}_5$. The metallic behavior gets interrupted at 11 K at which point ρ begins to increase down to 4.2 K. Then for T less than 4.2 K, it decreases slightly due to the magnetic ordering followed by a sharp decrease below T_{N1} at 3.8 K [Fig. 8(a), inset]. The reduction in ρ below ordered state/s is attributed to the reduction in spin disorder scattering. A similar low-temperature behavior is observed for $J \parallel a$. It is to be mentioned here, just above the ordered state, ρ for $J \parallel a$ decreases with increase in temperature and exhibits a minimum before it increases further with increase in temperature. This type of minimum in ρ has typically been attributed to magnetic frustration [20], however, in this case, there is no geometrical frustration in the lattice and still a minimum in resistivity is observed. A broad hump-like feature between 50 to 250 K can clearly be seen in ρ for $J \parallel a$ which is attributed to the CEF effects where higher-lying states are being populated as T increases [14]. The ratio of resistivity along c and a directions is found to be 1.6 at 300 K. The residual resistivity is high in $\text{Ho}_2\text{Re}_3\text{Si}_5$ along both the crystallographic directions. A similar high residual resistivity is observed in the isostructural Ce and $\text{Pr}_2\text{Re}_3\text{Si}_5$ and may be attributed to the disorder and/or defect present in the system [9]. The resistivity data clearly show a strong anisotropy in electrical transport properties in $\text{Ho}_2\text{Re}_3\text{Si}_5$.

The electrical resistivity varies in a complicated way with the application of magnetic field as we have already seen the complex magnetic phases in M_c (Fig. 4). The $\rho(T)$ for $J \parallel a$ and $\mu_0 H \parallel c$, namely, ρ_c is shown in Figs. 8(b) and 8(c). The

T_{N1} shifts to lower temperature from 3.8 to 2.7 K for fields up to 4 kOe. The T_{N2} is not discernible in ρ_c at low fields, while a new anomaly appeared at ~ 3.9 K at 2 kOe that might correspond to T_{N2} . This can be correlated with the enhanced feature of T_{N2} between 1 to 2 kOe in χ_c . The value of ρ_c significantly decreases below this transition, and only one transition at 3.8 K at 5.5 kOe is observed. Similarly, only one transition was seen in χ_c at 4 kOe [Figs. 3(b) and 3(c)]. This is because of the field-induced modification in the magnetic structure when $\text{Ho}_2\text{Re}_3\text{Si}_5$ enters in AFM2 phase. Furthermore, T_{N1} vanishes at 20 kOe. Between 8.7 and 12 kOe, there is no considerable shift. At 15 kOe, this broad transition shifts towards lower temperature. Such a low-temperature shift has also been observed in χ_c at 10.5 kOe. This transition wipes out at 15 kOe which is associated with the field-induced ferromagnetic state. Note that as the magnetic field increases from 1 to 4 kOe, residual resistivity increases which indicates that scattering of charge carriers increases due to enhanced spin fluctuations. Further increase in field, residual resistivity decreases due to suppression of spin fluctuation as the field-induced ferromagnetic state sets in Ref. [9]. The resistivity results are consistent with susceptibility data, and show that transport properties of $\text{Ho}_2\text{Re}_3\text{Si}_5$ are highly sensitive to the external magnetic field. With the field dependent studies of magnetic susceptibility and the electrical resistivity one can construct the magnetic phase diagram. However, it is challenging to construct a magnetic phase diagram because the two magnetic transitions are so close to each other and difficult to trace the field dependence of these transitions. In the supplemental material, we have constructed a tentative magnetic phase diagram from the field dependent magnetic susceptibility and electrical resistivity measurements [21]. More precise measurements are necessary to understand the complex magnetic behavior exhibited by $\text{Ho}_2\text{Re}_3\text{Si}_5$.

E. Conclusion

We have investigated the anisotropic magnetic properties in detail and constructed the magnetic phase diagram of $\text{Ho}_2\text{Re}_3\text{Si}_5$ single crystal using magnetic, electrical and thermal transport data. This compound shows two closely

spaced antiferromagnetic transitions at $T_{N1} \sim 3.8$ K and $T_{N2} \sim 4.2$ K. Magnetic susceptibility and magnetization show a complex magnetic structure in the field range 5 to 10.5 kOe, and finally it attains a field-induced ferromagnetic state at 15 kOe. These features are also reflected in field-dependent electrical resistivity and heat capacity. Three first-order field-induced metamagnetic transitions at 4.5, 10, and 15 kOe at 2 K have been observed. Hysteresis is completely suppressed and metamagnetic transitions become feeble at 3.5 K. These metamagnetic transitions are consistent with field-induced magnetic phases observed in magnetic susceptibility, resistivity and heat capacity. Further detailed studies of the magnetic

structure like neutron diffraction, will throw more light on the spin structure in $\text{Ho}_2\text{Re}_3\text{Si}_5$.

ACKNOWLEDGMENTS

The authors thank the Department of Atomic Energy (DAE), Government of India for the financial assistance. One of the authors Shovan Dan would like to thank SERB India (Grant No. PDF/2021/004624) for the financial assistance. Authors also acknowledge Jayesh Parmar and Vilas Mhatre, TIFR, Mumbai for EDX and XRD measurements, respectively.

-
- [1] M. Okawa, M. Matsunami, K. Ishizaka, R. Eguchi, M. Taguchi, A. Chainani, Y. Takata, M. Yabashi, K. Tamasaku, Y. Nishino, T. Ishikawa, K. Kuga, N. Horie, S. Nakatsuji, and S. Shin, *Phys. Rev. Lett.* **104**, 247201 (2010).
- [2] B. Shen, Y. Zhang, Y. Komijani, M. Nicklas, R. Borth, A. Wang, Y. Chen, Z. Nie, R. Li, X. Lu *et al.*, *Nature (London)* **579**, 51 (2020).
- [3] S. Ramakrishnan, N. G. Patil, A. D. Chinchure, and V. R. Marathe, *Phys. Rev. B* **64**, 064514 (2001).
- [4] P. Solokha, R. Freccero, S. De Negri, D. M. Proserpio, and A. Saccone, *Struct. Chem.* **27**, 1693 (2016).
- [5] H. Q. Ye, T. Le, H. Su, Y. N. Zhang, S. S. Luo, M. J. Gutmann, H. Q. Yuan, and M. Smidman, *Phys. Rev. B* **105**, 014405 (2022).
- [6] S. Ramakrishnan, A. Schönleber, T. Rekiş, N. van Well, L. Noohinejad, S. van Smaalen, M. Tolkiehn, C. Paulmann, B. Bag, A. Thamizhavel, D. Pal, and S. Ramakrishnan, *Phys. Rev. B* **101**, 060101(R) (2020).
- [7] Z. Hossain, H. Ohmoto, K. Umeo, F. Iga, T. Suzuki, T. Takabatake, N. Takamoto, and K. Kindo, *Phys. Rev. B* **60**, 10383 (1999).
- [8] V. K. Anand, Z. Hossain, and C. Geibel, *Phys. Rev. B* **77**, 184407 (2008).
- [9] S. Sanki, V. Sharma, S. Sasmal, V. Saini, G. Dwari, B. B. Maity, R. Kulkarni, R. Prakash Pandeya, R. Mondal, A. Lakshan, S. Ramakrishnan, P. Pratim Jana, K. Maiti, and A. Thamizhavel, *Phys. Rev. B* **105**, 165134 (2022).
- [10] S. Ramakrishnan, A. Schönleber, J.-K. Bao, T. Rekiş, S. R. Kotla, A. M. Schaller, S. van Smaalen, L. Noohinejad, M. Tolkiehn, C. Paulmann, N. S. Sangeetha, D. Pal, A. Thamizhavel, and S. Ramakrishnan, *Phys. Rev. B* **104**, 054116 (2021).
- [11] M. Nakashima, H. Kohara, A. Thamizhavel, T. D. Matsuda, Y. Haga, M. Hedo, Y. Uwatoko, R. Settai, and Y. Ōnuki, *J. Phys.: Condens. Matter* **17**, 4539 (2005).
- [12] H. F. Braun, *J. Less-Common Met.* **100**, 105 (1984).
- [13] J. Rodríguez-Carvajal, *Phys. B: Condens. Matter* **192**, 55 (1993).
- [14] M. A. Khan, Q. Zhang, J.-K. Bao, R. S. Fishman, A. S. Botana, Y. Choi, G. Fabbris, D. Haskel, J. Singleton, and J. F. Mitchell, *Phys. Rev. Mater.* **3**, 114411 (2019).
- [15] B. K. Cho, B. N. Harmon, D. C. Johnston, and P. C. Canfield, *Phys. Rev. B* **53**, 2217 (1996).
- [16] C. Detlefs, F. Bourdarot, P. Bulet, P. Dervenagas, S. L. Bud'ko, and P. C. Canfield, *Phys. Rev. B* **61**, R14916 (2000).
- [17] W. Zhang, C. Guo, D. Xie, M. Smidman, B. Hu, Y. Xia, Y. Liu, S. Tan, W. Feng, X. Zhu *et al.*, *Sci. Rep.* **8**, 7835 (2018).
- [18] M. T. Hutchings, *Solid State Phys.* **16**, 227 (1964).
- [19] K. W. H. Stevens, *Proc. Phys. Soc. A* **65**, 209 (1952).
- [20] Z. Wang, K. Barros, G.-W. Chern, D. L. Maslov, and C. D. Batista, *Phys. Rev. Lett.* **117**, 206601 (2016).
- [21] See Supplemental Material at <http://link.aps.org/supplemental/10.1103/PhysRevMaterials.6.124406> for the tentative magnetic phase diagram of $\text{Ho}_2\text{Re}_3\text{Si}_5$ constructed from the field dependent magnetic susceptibility, electrical resistivity, and heat capacity data.